C Journal of Carbon Research

MDPI

Article

Release of Bioactive Molecules from Graphene Oxide-Alginate Hybrid Hydrogels: Effect of Crosslinking Method

Lorenzo Francesco Madeo [1,*], Manuela Curcio [2], Francesca Iemma [2], Fiore Pasquale Nicoletta [2], Silke Hampel [1] and Giuseppe Cirillo [2,*]

[1] Leibniz Institute of Solid State and Material Research Dresden, 01069 Dresden, Germany
[2] Department of Pharmacy Health and Nutritional Science, University of Calabria, 87036 Rende, Italy
* Correspondence: l.f.madeo@ifw-dresden.de (L.F.M.); giuseppe.cirillo@unical.it (G.C.); Tel.: +49-351-4659883 (L.F.M.); +39-0984-493208 (G.C.)

Abstract: To investigate the influence of crosslinking methods on the releasing performance of hybrid hydrogels, we synthesized two systems consisting of Graphene oxide (GO) as a functional element and alginate as polymer counterpart by means of ionic gelation (physical method, H^P_{A-GO}) and radical polymerization (chemical method, H^C_{A-GO}). Formulations were optimized to maximize the GO content (2.0 and 1.15% for H^P_{A-GO} and H^C_{A-GO}, respectively) and Curcumin (CUR) was loaded as a model drug at 2.5, 5.0, and 7.5% (by weight). The physico-chemical characterization confirmed the homogeneous incorporation of GO within the polymer network and the enhanced thermal stability of hybrid vs. blank hydrogels. The determination of swelling profiles showed a higher swelling degree for H^C_{A-GO} and a marked pH responsivity due to the COOH functionalities. Moreover, the application of external voltages modified the water affinity of H^C_{A-GO}, while they accelerated the degradation of H^P_{A-GO} due to the disruption of the crosslinking points and the partial dissolution of alginate. The evaluation of release profiles, extensively analysed by the application of semi-empirical mathematical models, showed a sustained release from hybrid hydrogels, and the possibility to modulate the releasing amount and rate by electro-stimulation of H^C_{A-GO}.

Keywords: crosslinking methods; electro-responsivity; graphene oxide; hybrid hydrogels; sodium alginate; sustained release

Citation: Madeo, L.F.; Curcio, M.; Iemma, F.; Nicoletta, F.P.; Hampel, S.; Cirillo, G. Release of Bioactive Molecules from Graphene Oxide-Alginate Hybrid Hydrogels: Effect of Crosslinking Method. *C* **2023**, *9*, 8. https://doi.org/10.3390/c9010008

Academic Editor: Francois Normand

Received: 30 November 2022
Revised: 22 December 2022
Accepted: 4 January 2023
Published: 8 January 2023

1. Introduction

Over the last decades, growing interest has been directed to the development of high-performing drug delivery devices able to either transport bioactive compounds to a target site without the insurgence of severe side-effects [1–3], or control the release profile keeping the drug within a desired concentration range [4,5]. Within this research field, Graphene oxide (GO) has attracted much attention due to its unique and superior surface properties, such as a highly specific surface area, an affinity for biologically active molecules, and the possibility for easy and versatile chemical derivatization [6–8]. Moreover, the high water affinity, relatively low cytotoxicity, and amphiphilic character of GO were widely explored for the fabrication of hybrid materials coupling such favorable features with those of hydrogel systems [9–11]. Hydrogels, indeed, possess high similarities (both structural and compositional) to the extracellular matrix (ECM), as well as the ability to promote cell attachment, migration, and proliferation by virtue of their three-dimensional porous structure [12,13]. Such materials were widely proposed for different applications in biomedicine, with the treatment of skin wounds being one of the most investigated research fields [14–16].

Hydrogel dressings, indeed, are able to maintain a moist wound environment, cool the wound surface, and promote oxygen; thus the healing process, with the further advantage to allow the release of loaded agents to be finely tuned according to the therapeutic needs [17–20].

The crosslinking methods used for the fabrication of hydrogels greatly influence the performance of the final hydrogel systems [21]: physical crosslinking is expected to carry out to safe materials owing to the absence of any residues of unreacted chemical species, also confer self-healing property and shape adaptability, while chemical methods show the advantage of higher mechanical strength and stability [22], although the use of competitive molecules in the case of dissolvable hydrogels can lead to potential toxic effects [23]. The two methods are often combined to couple the biomechanical activity needed in the early stage of the healing process with the multiple biochemical functions required to promote wound healing after wound closure. As an example of these findings, poly(N-isopropylacrylamide) was combined with quaternized chitosan to benefit from the mechanical strength of acrylic polymers and the adhesion property of chitosan derivative [24]. Similarly, a multi-layered first-aid burn wound patch was obtained using a physical interpenetrating hydrogel consisting of a chemically crosslinked polyacrylamide-chitosan hydrogel and poly(vinyl alcohol) layers [25]. In another approach, glutaraldehyde was used as a chemical crosslinker to enhance the stability of a physical hydrogel composed of poly(3,4-ethylenedioxythiophene): polystyrene sulfonate nanofibrils [26].

Due to its non-toxicity, biocompatibility, and biodegradability, sodium alginate (Alg) is an interesting starting material for the formulation of biomedically oriented hydrogels [27–29].

From a chemical point of view, Alg, the water-soluble sodium salt of alginic acid, is an anionic polysaccharide extracted from certain brown seaweeds [30,31]. It comprises homopolymer and heteropolymer blocks of linearly linked α-(1-4)-L-guluronic acid (G) and β-(1-4)-D-mannuronic acid (M) residues [32]. Although its advantageous features, Alg-based networks suffer from low mechanical strength and lack of interlinking with cells, and thus bioglasses, ceramics, and polymers, as well as carbon nanomaterials are proposed as functional additives [33–36].

Among others, literature in the biomedical field is plenty of Alg/GO hybrid hydrogels proposed for the treatment of cancer, bacterial infections, and cardiovascular and gastrointestinal diseases [37–39]. Alg/GO hydrogels can be synthesized by means of either ionic gelation with divalent cations (e.g., Ca^{2+}, Mg^{2+}, Sr^{2+}) [40–42], or by chemical reaction with suitable crosslinkers (e.g., glutaraldehyde, adipic acid dihydrazide, and poly (ethylene glycol)-diamine)) [43–45].

Our previous research activity explored the feasibility of coupling GO and Alg features via both chemical and physical crosslinking. In the first case, we formulated a performing platform to either facilitate the crystallization of biologically active protein (e.g., lysozyme) under oxidative stress or provide its electro-responsive release [46]. On the other hand, the use of Ca^{2+} ionic crosslinking was investigated for modulating the release of Curcumin as bioactive agent in the treatment of Squamous Cell Carcinoma [47]. The results of both approaches proved that the performance of the hybrid materials is strictly dependent on their composition, and that the need for co-monomer species in the synthesis of the chemical hydrogels hinders the direct exposure of GO on the material surface, which is mainly confined within the hydrogel core.

Here, we aim to elucidate in detail the effect of the different crosslinking strategies (physical and chemical), by comparing the delivery performance of Alg/GO hybrid hydrogels synthesized through (i) Ca^{2+} gelation (H^{P}_{A-GO}) and (ii) radical co-polymerization (H^{C}_{A-GO}) in the presence of acrylate monomers/crosslinkers. Curcumin (CUR) was selected as a model drug and the release profiles were evaluated in the presence of electric stimulation, in order to underline how the crosslinking strategy influenced the possibility to transfer the intrinsic properties of the carbon nanostructure to the final delivery device.

2. Materials and Methods

2.1. Synthesis of Ionically Crosslinked Hybrid Hydrogels

The reaction mixture was prepared as previously reported [47], by adding a 2.0% amount (w/w) of GO to a 2.0% (w/v) Alg solution in double distilled water (ddH_2O), stirring for 15 min and then sonicating by a horn-tipped ultrasonic probe (20% amplitude,

BANDELIN Electronic GmbH, Berlin, Germany) for other 15 min. Thereafter, in separate experiments, selected amounts of a 0.5% (*w*/*v*) CUR ethanol solution were added to one such mixture to reach CUR to initial reaction feed ratios of 2.5, 5.0, and 7.5% (*w*/*w*).

The platform for the ionic crosslinking was prepared by heating up until boiling a solution of 1.0% *w*/*v* agar and 0.2 M calcium chloride in ddH_2O and then cooling it into a Petri dish. Then, the reaction mixture was gently poured onto the agar platform and left crosslinking at 40 °C for 2 h. The obtained H^P_{A-GO} hydrogel was peeled off the agar gel, washed in ddH_2O to remove unreacted species, and dried at 40 °C for 12 h. The same approach was used for the preparation of unloaded and blank samples.

All chemicals were purchased from Merck/Sigma Aldrich, Darmstadt, Germany.

2.2. Synthesis of Chemically Crosslinked Hybrid Hydrogels

According to a previously reported method [46], for the synthesis of H^C_{A-GO} hydrogels, a pre-polymerization feed was prepared by adding 184 mg HEA and 196 mg PEGDMA to a 1.15% GO (*w*/*w*) dispersion in Alg obtained as reported in paragraph 2.1 and purging with gaseous nitrogen for 20 min. A 10% (*w*/*w*) ammonium persulfate was inserted as the initiator system and the mixture reacted at 40 °C after being placed between two 5.0 × 5.0 cm^2 glass plates, separated with a Teflon spacer (0.6 mm) and brought together by binder clips. The obtained H^C_{A-GO} hydrogel was washed in ddH_2O to remove unreacted species and dried at 40 °C for 12 h. The same approach was used for the preparation of unloaded and blank samples.

All chemicals were from Merck/Sigma Aldrich, Darmstadt, Germany.

2.3. Instrumentation

An SDT Q600 (TA Instruments, Hüllhorst, Germany) was used for the thermogravimetric analysis (TGA) using the following conditions: 10 mg initial sample weight, 10 mL min^{-1} N_2 flow, 25–800 °C temperature range, 10 °C min^{-1} heating rate.

A NOVA NanoSEM 200 [0–30 kV] (Thermo Fisher Scientific, Hillsboro, OR, USA) was used to record the scanning electron microscope (SEM) images of samples after deposition of samples onto self-adhesive, conducting carbon tape (Plano GmbH, Wetzlar, Germany).

2.4. Determination of Weight Variation in Water Media

The water affinity of blank and hybrid hydrogels was evaluated by immersing weighted specimens of each sample (~5.0 cm^2) in the swelling media, consisting of either acetate (10^{-4} M, pH 5.5) or phosphate-buffered saline (PBS) solution (10^{-4} M, pH 7.4) at 37 °C. After incubation for predetermined time intervals, samples were weighed after the surface moisture removal by blotting with a tissue. The results were expressed as weight variation percentage (*WV*) according to the following Equation (1):

$$WV = \frac{W_s - W_d}{W_d} \times 100 \quad (1)$$

Here, W_d and W_s represent the weight of samples in the dried and swollen state, respectively.

The same experiments were performed upon application of an external electric field at 12, 24, and 48 V.

All chemicals were purchased from Merck/Sigma Aldrich, Darmstadt, Germany.

2.5. Determination of In Vitro Release Profiles

For the determination of the in vitro CUR release profiles, the dissolution method was used [48]. In separate experiments, weighted specimens of ~1 cm^2 of loaded hydrogels were immersed in 10 mL releasing media consisting of a mixture (4/6 vol/vol) of ethanol and either acetate- (10^{-4} M, pH 5.5) or phosphate-buffered saline (PBS, 10^{-4} M, pH 7.4) at 37.0 ± 0.1 °C. 1.0 mL release medium was withdrawn at predetermined time intervals, filtered with Iso-DiscTM Filters PTFE 25-4 25mm×0.45 μm (Merck/Sigma Aldrich,

Darmstadt, Germany), and replaced with fresh release medium to ensure sink conditions throughout the experiment. The amount of released CUR, determined by UV–Vis analysis on an Evolution 201 spectrophotometer (ThermoFisher Scientific, Hillsboro, OR, USA) operating with 1.0 cm quartz cells set at 430 nm, was expressed according to the following Equation (2) using a calibration curve recorded in the same conditions:

$$CUR\ release = \frac{M_t}{M_0} \quad (2)$$

where M_t and M_0 are the CUR amount (mg) detected at time t and loaded into the hydrogels, respectively.

The same experiments were performed upon the application of an external electric field at 12, 24, and 48 V.

All chemicals were purchased from Merck/Sigma Aldrich, Darmstadt, Germany.

2.6. Statistical Analyses

All results were expressed as means ± SD (standard deviation), obtained over three independent experiments

3. Results and Discussion

In this investigation, Alg/GO hybrid hydrogels were synthesized by exploiting both the physical and chemical crosslinking approaches. Physical crosslinking was achieved by using an agar gel platform for controlling the homogeneous diffusion of calcium ions within the Alg solution containing well-dispersed GO (H^P_{A-GO}), while in the latter case, the system consisted of an acrylate network containing Alg and GO as functional additives (H^C_{A-GO}).

Both approaches are well-known in the literature, as were used by our research group for the fabrication of valuable platforms for modulating the release of small- and macromolecules of biological interests, as well as for controlling the crystallization of bioactive proteins [46,47].

Here, with the aim of comparing the performance of the two systems, we used Curcumin (CUR) as a model therapeutic agent, because of either its chemical features (e.g., hydrophobic character requiring suitable carrier for safe and effective administration) or its fascinating biological properties (e.g., antioxidant, antimicrobial, anti-inflammatory, anticancer), which generally characterize such compounds in medicine.

3.1. Synthesis of Physically Crosslinked Hydrogels and Curcumin Loading

At first, based on our previous work, the physical system (H^P_{A-GO}) was synthesized via Ca^{2+}-induced ionic gelation of an Alg/GO aqueous mixture (Figure 1).

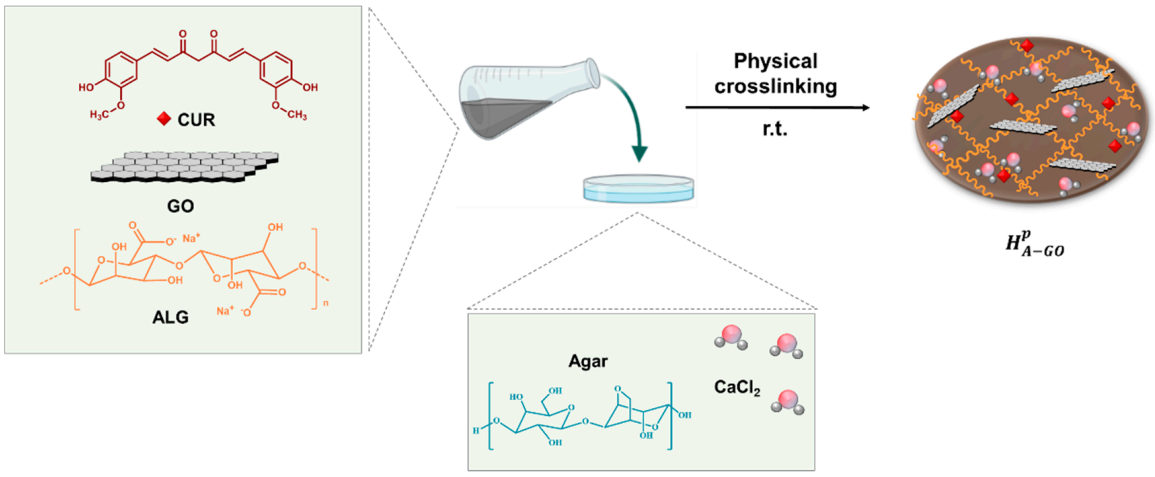

Figure 1. Schematic representation of the preparation of H^P_{A-GO} hydrogels.

As explained elsewhere [47], the used GO-to-Alg ratio (2.0% by weight) represents the highest amount of GO that can be homogeneously incorporated within the hydrogel network: an increase in the GO content carried out to the formation of large GO aggregates (diameter > 750 nm) due to unstable dispersion, while lower GO content was discharged to avoid the formation of poorly effective delivery vehicles. Moreover, it was proved that the addition of a CUR solution in ethanol to the reaction feed before inducing the ionic crosslinking is a valuable approach for obtaining the loaded samples ($Cur@H^{P}_{A-GO}$). In detail, three CUR different amounts (by weight) were loaded, namely 2.5, 5.0, and 7.5%, since higher amounts were found to be not dispersible in the Alg/GO dispersion.

3.2. Synthesis of Chemically Crosslinked Hydrogels and Curcumin Loading

The chemical system (H^{C}_{A-GO}) was synthesized via radical polymerization of GO dispersion in Alg in the presence of GO, hydroxyethyl acrylate (HEA) and polyethylene glycol dimethacrylate 750 (PEGDMA) acting as plasticizing and crosslinking monomers, respectively (Figure 2).

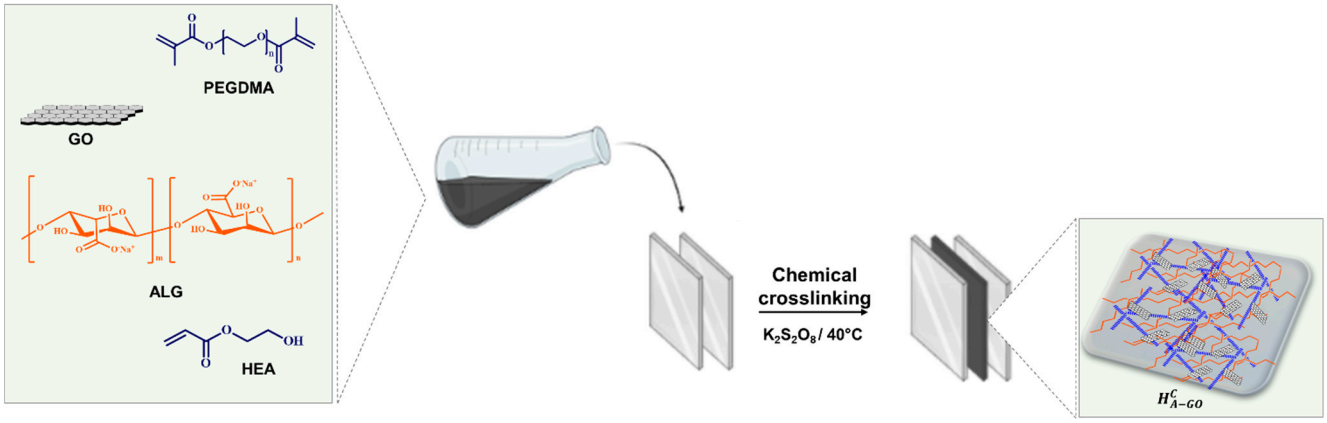

Figure 2. Schematic representation of the preparation of H^{C}_{A-GO} hydrogels.

As reported in the literature, the formation of the polymer network is attributed to the ability of oxygen-rich functionalities of both Alg (e.g., hydroxy and carboxy) and GO (e.g., epoxide, phenol, hydroxy, and carboxy) to be covalently incorporated in growing polymer chains as transfer and/or terminating agents [46]. By this approach, the higher amount of GO incorporated within the polymer network is 1.15%: although more GO can be dispersed in the pre-polymerization feed, no homogenous materials were obtained in such conditions. Thus, to compare samples with the highest amount of GO, we used this composition for the fabrication of H^{C}_{A-GO}.

For the loading of the bioactive agent, we exploited a soaking procedure, reaching a maximum CUR content of 4.5% (by weight). Subsequently, to increase the loading percentage, we moved to a different approach involving the incorporation of the polyphenol within the pre-polymerization feed. As reported for $Cur@H^{P}_{A-GO}$, also in this case we tested three CUR contents (2.5, 5.0, and 7.5% by weight) since higher amounts were found to interfere with the growth of the polymer chains (un-effective hydrogel formation) due to the well-known CUR scavenging effect [49].

3.3. Characterization of Hydrogel Systems

Before testing the performance of the synthesized materials as topical CUR delivery vehicles, a physico-chemical characterization procedure was employed to compare (H^{P}_{A-GO}) and (H^{C}_{A-GO}) in terms of surface morphology, thermal stability (thermogravimetric analyses), and electro-responsivity (determination of water affinity in the presence or absence of an external electric field). The sample consistency did not allow the stress-strain measurements, since they became brittle and broke as soon as they were attached to a clamp.

H^P_{A-GO} and H^C_{A-GO} hybrid hydrogels showed a rough surface, with GO appearing as dots embedded within the polymer network (Figure 3a,b).

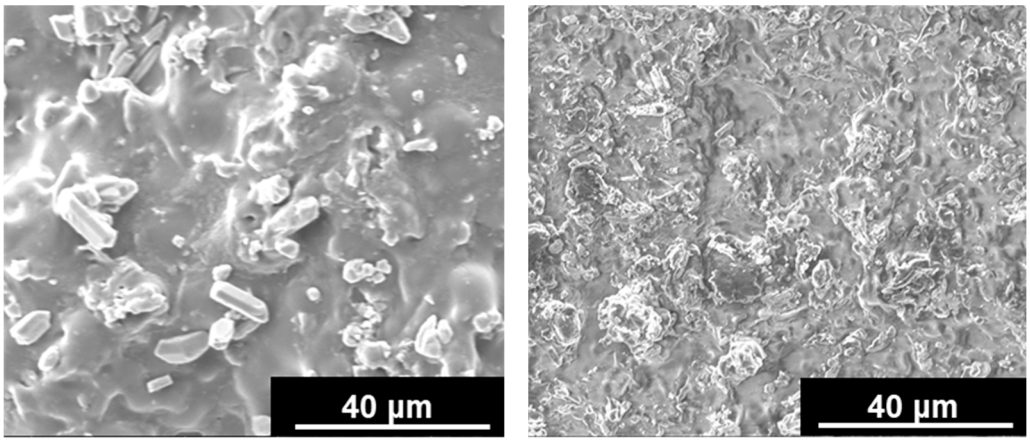

Figure 3. SEM images of (**a**) H^P_{A-GO} and (**b**) H^C_{A-GO} showing the GO sheet incorporated into the hybrid materials and emerging from the surface.

As far as the thermal properties are concerned, TGA measurements were performed in the range of 50–800 °C in order to evaluate the effect of each component on the thermal behavior (Figure 4a,b).

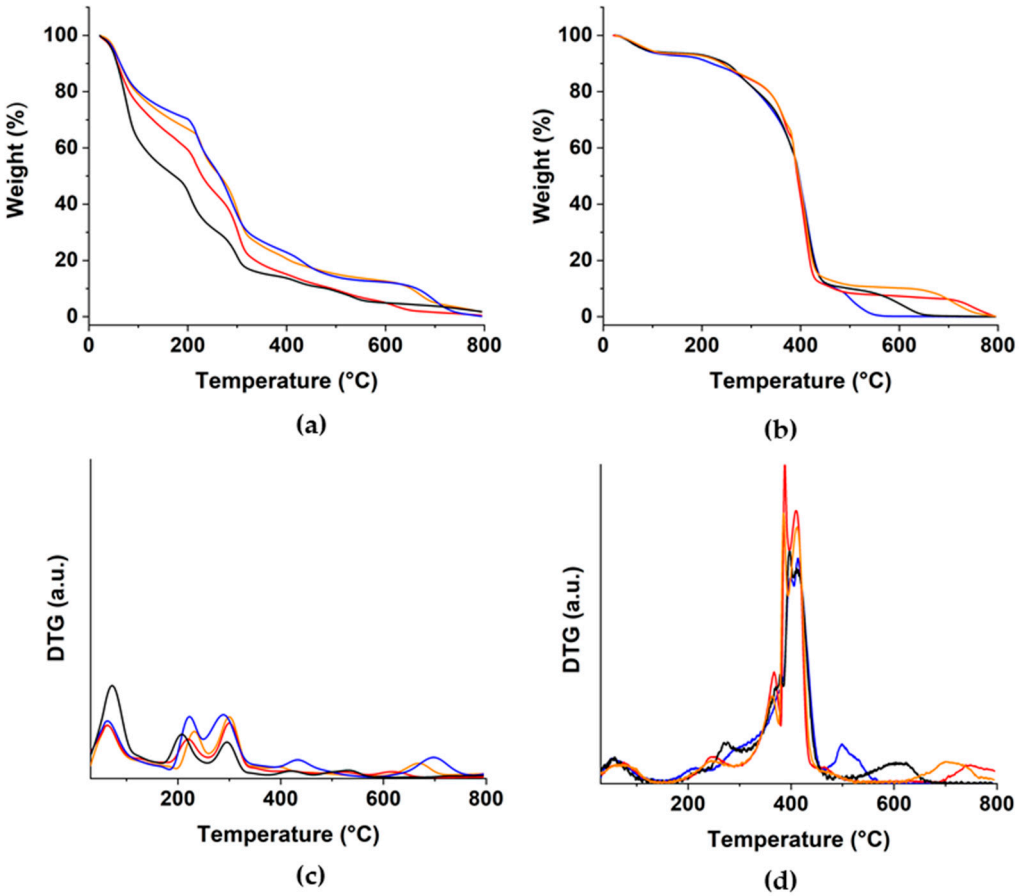

Figure 4. (**a**,**b**) TGA and (**c**,**d**) DTG curves of (**a**,**c**) H^P_A (blue line), H^P_{A-GO} (black line), $CUR@H^P_A$ (red line), $CUR@H^P_{A-GO}$ (orange line), and (**b**,**d**) H^C_A (blue line), H^C_{A-GO} (black line), $CUR@H^C_A$ (red line), $CUR@H^C_{A-GO}$ (orange line). Panel (**a**) adapted from [47].

The chemical crosslinking was able to confer higher thermal stability compared to the ionic gelation, as per DTG curves (Figure 4c,d) with the main weight loss occurring at higher temperatures in H^C_{A-GO} (350–450 °C) vs. H^P_{A-GO} (200–300 °C). Similarly, due to the lower strength of the Ca^{2+} crosslinking points, the weight loss located at around 100 °C (elimination of the free water) is more evident in H^P_{A-GO}. At around 300 °C, the signals related to the decomposition of free Alg chains were detected for H^P_{A-GO}, while H^C_{A-GO} showed no significant weight loss at this temperature range since the polysaccharide chains were covalently inserted into a stabilizing acrylate network. The degradation phenomena occurring at 400 °C were related to the release of CO_2 as a consequence of either the fracture of glycoside bonds, the decarbonylation of alginate chains (H^P_{A-GO}), or the decomposition of the HEA and PEGDMA residues (H^C_{A-GO}) [50,51]. It should be pointed out that in both cases, the presence of GO counteracted the degradation phenomena, resulting in lower weight loss compared to blank samples. Finally, the incorporation of CUR contributed to a further enhancement of the thermal stability of the hydrogel structure.

Since water affinity is a key requirement for any material proposed for interactions with living tissues, H^P_{A-GO} and H^C_{A-GO} were characterized by the determination of swelling behavior in water media.

Such determination was performed either in the presence or in the absence of the application of an external electric field at 12, 24, and 48 V in order to evaluate how the different synthetic approaches affected the electric conductivity of GO when inserted in the hydrogel networks. Moreover, since the application of the external voltage is expected to influence the water affinity behavior via modulation of the ionization degree [52], the weight variation was measured at two pH conditions (pH 5.5 and pH 7.4), mimicking an acidic and a physiological environment, respectively. For a better discussion of the experimental data, we introduced the weight ratio parameter (*We*) as follows (Equation (3)):

$$W_e = \frac{WV_v - WV_{0v}}{WV_{0v}} \times 100 \quad (3)$$

where WV_v and WV_{0v} were the weights of samples after 24 h incubation at the selected (12, 24, and 48 V) voltage and 0 V, respectively.

From the analysis of the reported data, it is clearly evident that chemical and physical hydrogels showed totally different behavior.

At first, it should be highlighted that negligible variation of *WV* upon application of the external voltage was noticed for H^C_A sample at both pH values, as expected for blank hydrogels with low electric conductivity (Table 1) [53].

On the other hand, significant changes (W_e values > 14.7 in all cases) in the swelling behaviors were detected for H^C_{A-GO}, as a consequence of the high electro-responsivity of the hybrid hydrogel due to the presence of the GO sp^2 carbon layer [54]. In detail, two main phenomena should be considered, namely the ionization of the COOH functionalities on Alg and GO, as well as the rearrangement of mobile ions between the inner core and outer surface of the sample, with the movements of ions to the opposite electrodes generating osmotic pressure and deformation of the hydrogel network [55]. As extensively discussed elsewhere [46], the application of low voltages (12 and 24 V) induced a prevalent ionization effect, triggering the swelling of the hydrogels, while at higher values (48 V), the osmotic pressure became the prevalent phenomena, with the reduction of S_e values due to a more evident network deformation. Moreover, the slight differences recorded at acidic vs. physiological conditions (higher W_e values at pH 5.5) could be related to the different ionization degrees of carboxylic groups in the two environments. At physiological pH, a larger number of COOH groups already underwent dissociation, and thus the electric stimulation was less effective in varying the carboxylate to carboxylic groups balance within samples.

Table 1. Weight variation in water media of blank and hybrid hydrogels after 24 h incubation at pH 5.5 and 7.4 in the absence or presence of external voltages.

Hydrogel	pH	Voltage (V)	WV (%)	W_e (%)
H_A^C	5.5	0	221	
		12	224	1.4
		24	227	2.7
		48	230	4.1
	7.4	0	401	
		12	411	2.5
		24	406	1.2
		48	409	2.0
H_{A-GO}^C	5.5	0	258	
		12	296	14.7
		24	384	48.8
		48	348	34.9
	7.4	0	517	
		12	651	25.9
		24	691	33.7
		48	673	30.2
H_A^P	5.5	0	251	
		12	208	−17.1
		24	187	−25.4
		48	164	−34.6
	7.4	0	554	
		12	202	−63.5
		24	152	−72.5
		48	124	−77.6
H_{A-GO}^P	5.5	0	157	
		12	147	−6.3
		24	138	−12.2
		48	114	−27.4
	7.4	0	436	
		12	309	−29.1
		24	252	−42.2
		48	197	−54.8

As far as physical hydrogels are concerned, the interference between calcium and sodium ions after long-time incubation (e.g., 144 h) carried out the disruption of the crosslinking points, with the destabilization of the H_{A-GO}^P structure and the partial dissolution of alginate. As a consequence, a reduction in the swelling degree was observed, which can be quantified by the determination of a degradation parameter (D_d) according to the following Equation (4):

$$D_d = \frac{WV_{0v}^{144h} - WV_v^{24h}}{WV_{0v}^{144h}} \times 100 \quad (4)$$

where WV_v^{24h} and WV_{0v}^{144h} were the weights of samples after 24 (at selected voltage) and 144 (at 0 V) h incubation, respectively.

Such degradation was more evident at pH 7.4 (higher ions movement) and significantly reduced in H_{A-GO}^P (D_d of 141 and 257 at pH 5.5 and 7.4, respectively) vs. H_A^P (D_d of 17 and 38 at pH 5.5 and 7.4, respectively) samples due to the stabilizing effect of GO. For both H_{A-GO}^P vs. H_A^P hydrogels, the application of the external voltage was found to favor the Ca^{2+}/Na^+ exchange, thus promoting hydrogel degradation. The resulting *We* values were thus the results of multiple phenomena, including the ionization of COOH groups, the insurgence of osmotic pressure between the core and the surface of samples, as well as the

loss of crosslinking points. In all conditions, the latter is the predominant effect (negative S_e values in physical hydrogels), although to a different extent.

Finally, the comparison of H^P_{A-GO} and H^C_{A-GO} behavior showed higher water affinity for chemically crosslinked materials, and this can be ascribed to the presence of high hydrophilic monomers and to the lower GO content per unit of mass.

3.4. Curcumin Delivery Behavior of Hydrogel Systems

Due to the hydrophobic character of CUR, the composition of the release media should be finely tuned by adding a proper solubilizing agent. Here, we choose ethanol according to the literature work suggesting the use of this co-solvent for assessing the CUR release in the case of in vitro studies on U251 glioma cells [56], and for the formulation of conventional anticancer drugs [57].

Moreover, since the release of any loaded molecule within a delivery vehicle can be considered as an equilibrium partition phenomenon between the two phases represented by the carrier and the releasing media, respectively, it strongly depends on both the drug-to-carrier interaction and the drug concentrations [58]. In these conditions, reversible first- or second-order release can be hypothesized (Equations (5) and (6)):

$$\frac{M_t}{M_0} = F_{max}(1 - e^{-(\frac{k_R}{F_{max}})t}) \quad (5)$$

$$\frac{M_t}{M_0} = \frac{F_{max}(e^{2(\frac{k_R}{\alpha})t} - 1)}{1 - 2F_{max} + e^{2(\frac{k_R}{\alpha})t}} \quad (6)$$

k_R was the release rate constant, F_{max} the maximum amount of released drug (M_t/M_0), while α represented the physico-chemical affinity of the drug towards the solvent vs. the carrier phases and can be measured by the following Equation (7):

$$\alpha = \frac{F_{max}}{1 - F_{max}} \quad (7)$$

Based on this theory, the drug release occurred only when $\alpha > 0$.

The evaluation of R^2 values (Table 2) showed that the release data from H^P_A/H^P_{A-GO} data can be better fitted with the reversible second-order model ($R^2 > 0.90$), while the first-order model was more suitable for describing the release from H^C_A/H^C_{A-GO}.

Table 2. Fitting parameters for CUR release from hybrid (H^C_{A-GO} and H^P_{A-GO}) and blank (H^C_A and H^P_A) hydrogels.

Hydrogel	CUR Loading (wt%)	Reversible First Order			Reversible Second Order		
		R^2	F_{max}	α	R^2	F_{max}	α
H^P_A	2.5	0.8074	-	-	0.9105	0.60	1.51
	5.0	0.7954	-	-	0.9471	0.99	99
	7.5	0.6877	-	-	0.9322	0.99	99
H^P_{A-GO}	2.5	0.7688	-	-	0.9386	0.39	0.64
	5.0	0.6992	-	-	0.9112	0.80	4.01
	7.5	0.7598	-	-	0.9054	0.92	11.5
H^C_A	2.5	0.9322	0.99	99	0.8877	-	-
	4.5 *	0.9547	0.99	99	0.9258	-	-
	5.0	0.9471	0.99	99	0.8954	-	-
	7.5	0.9954	0.98	53.35	0.9411	-	-
H^C_{A-GO}	2.5	0.9054	0.92	11.50	0.8598	-	-
	4.5 *	0.9479	0.94	99	0.9025	-	-
	5.0	0.9112	0.80	4.01	0.8992	-	-
	7.5	0.9833	0.45	0.8	0.9584	-	-

* Soaking procedure.

It should be underlined that, as reported in our previous work [47], the release from physically crosslinked hybrid hydrogels loaded with CUR ratio of 5.0 and 7.5% (by weight) were characterized by high burst releases, with M_t/M_0 becoming higher than 0.70 after the first 2 h of incubation (F_{max} of 0.80 and 0.92, respectively).

In H^C_{A-GO} case, the loading procedure greatly affected the release behavior. A huge burst release (F_{max} > 0.9 reached after 3 h incubation) was recorded for samples prepared by soaking procedure, probably as a result of the confinement of the drug to carrier interaction to the surface of the hydrogels. For this reason, we considered a different approach based on the insertion of CUR in the pre-polymerization feed and its subsequent incorporation within the growing hydrogel network. In these conditions, it was possible to obtain not only higher loading percentages (up to 7.5%), but a sustained release. Samples loaded with a low CUR content (e.g., 2.5 and 5.0%) were characterized by a high drug-to-carrier affinity (low α values), resulting in very low F_{max} values (<0.10) recorded even after 144 h incubation.

The loading of H^P_{A-GO} and H^C_{A-GO} samples with 2.5 and 7.5% CUR, respectively, led to more interesting release profiles (Figure 5).

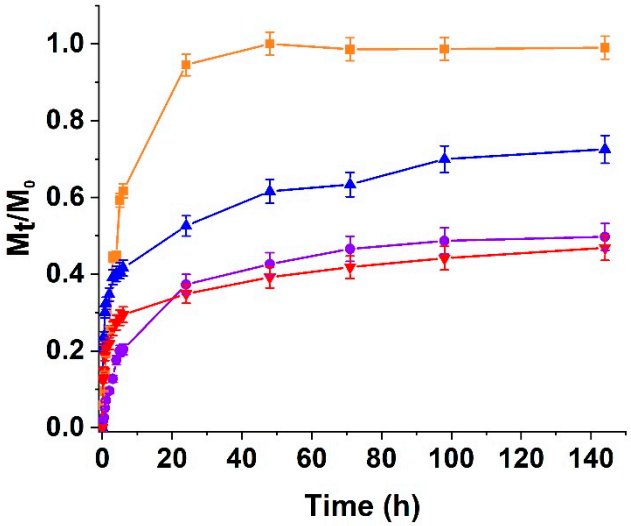

Figure 5. CUR release from H^P_A (blue line), H^P_{A-GO} (red line), H^C_A (orange line) and H^C_{A-GO} (violet line) as a function of time.

The high and effective interactions between the sp^2 carbon layer of GO and the aromatic ring of CUR were responsible for a sustained release from H^P_{A-GO}, with F_{max} value of 0.39 after 144 h incubation. The amount of released CUR was found to be significantly higher in the case of H^P_A (F_{max} of 0.60) due to the absence of the carbon nanostructure.

As expected, the presence of GO within the hydrogel network conferred higher affinity towards the bioactive agent to H^C_{A-GO} as well. In particular, we recorded F_{max} values of 0.45 and 0.98 for H^C_{A-GO} and H^C_A, respectively, higher than those obtained for H^P_{A-GO} and H^P_A, as a consequence of the interference of CUR with the polymerization of acrylate monomers.

Although the release from bio-erodible matrices (H^P_A and H^P_{A-GO}) is better modelized by different kinetic equations assuming that the rate is proportional to the surface area of the device changing with time [59], for a direct comparison of the release mechanisms and to highlight the effect of the different crosslinking method on the release parameters, in this work we applied the classical kinetic models available in the literature [60,61] to the release data within the experimental time (24 h) where degradation of polymer chains was almost negligible.

A steady state profile, with the release kinetics being independent of the drug concentrations, is evoked when experimental data can be fitted by zero-order Equation (8) [62]:

$$\frac{M_t}{M_0} = k_0 t \tag{8}$$

When the driving force of the release is the difference between the drug concentration inside and outside the dosage form, a first-order kinetics model can be applied (Equation (9)) [63]:

$$\frac{M_t}{M_0} = a\left(1 - e^{-k_1 t}\right) \quad (9)$$

Ritger-Peppas [61] and Peppas-Sahlin [64] equations represent semiempirical "power law" models assuming exponential proportionality between the amount of released drug and time. In the first case (Equation (10)), the exponent describes the release mechanism as Fickian diffusion ($n \leq 0.50$ for hydrogel films) or anomalous transport processes ($0.50 < n < 1.0$):

$$\frac{M_t}{M_0} = k_P t^n \quad (10)$$

The Peppas-Sahlin model (Equation (11)) allows the quantification of Fickian (k'_S) and anomalous phenomena (k''_S) contributions over the releasing kinetics:

$$\frac{M_t}{M_0} = k'_S t^m + k''_S t^{2m} \quad (11)$$

k_0, k_1, k_P, k'_S, and k''_S represent the constants of zero-order: first-order, Ritger-Peppas, Fickian diffusion, and anomalous diffusion kinetics, t the release time, a and n,m the first order, and Ritger-Peppas release coefficients, respectively.

In all cases, the nonlinear equations were applied to avoid the logarithm linearization approach resulting in distortions of the error distributions, and the data collected in Table 3.

Table 3. Kinetic parameters for CUR release from hybrid (H^C_{A-GO} and H^P_{A-GO}) and blank (H^C_A and H^P_A) hydrogels.

Hydrogel	Zero Order		First Order		Ritger-Peppas				Peppas-Sahlin			
	R^2	k_1 (10^{-3})	R^2	k_2	R^2	k_P	n	R^2	m	k'_S	k''_S (10^{-2})	$\frac{k'_S}{k''_S}$
H^P_A	0.692	9.36	0.794	0.52	0.996	0.29	0.19	0.998	0.21	0.31	1.7	18
H^P_{A-GO}	0.690	6.02	0.826	0.38	0.993	0.19	0.19	0.997	0.24	0.20	2.0	10
H^C_A	0.565	1.07	0.995	0.17	0.950	0.31	0.28	0.967	0.49	0.26	1.57	17
H^C_{A-GO}	0.734	0.50	0.985	0.11	0.924	0.11	0.34	0.988	0.54	0.08	0.34	23

It is clearly evident that the steady-state model (Equation (8)) was not suitable for describing the CUR release in all cases.

For physically crosslinked hydrogels, the diffusion of CUR molecules through the swollen hydrogel matrix is the main phenomena involved in the drug release, with R^2 values lower than 0.85 recorded for first-order kinetics (Equation (9)). On the other hand, data obtained from H^C_A and H^C_{A-GO} can be fitted by both Equations (9) and (10) ($R^2 > 0.90$ in all cases), meaning that the drug partition between the hydrogel and the releasing media phases should be considered together with its diffusion from swollen delivery vehicles.

The suitability of Equation (10) in describing the release from both chemical and physical hydrogels was thus used for a direct comparison between them, in order to underline the effect of the crosslinking method on the delivery profile. At first, it should be noted that although possessing the lowest swelling degree at physiological pH, H^P_{A-GO} was characterized by a faster release profile than H^C_{A-GO} (k_P of 0.19 vs. 0.11), further confirming that the hydrogel swelling cannot be considered the sole cause of the release mechanism. Moreover, the analysis of the Peppas-Sahlin parameters showed that the Fickian diffusion is the main phenomena involved in the release ($\frac{k'_S}{k''_S} \geq 10$), with more anomalous effects detected in H^P_{A-GO}, probably because of the higher GO content.

Moreover, the stability of H^C_{A-GO} hydrogels systems upon application of an external electric field allowed the modulation of the release behavior by varying the applied voltage (Figure 6).

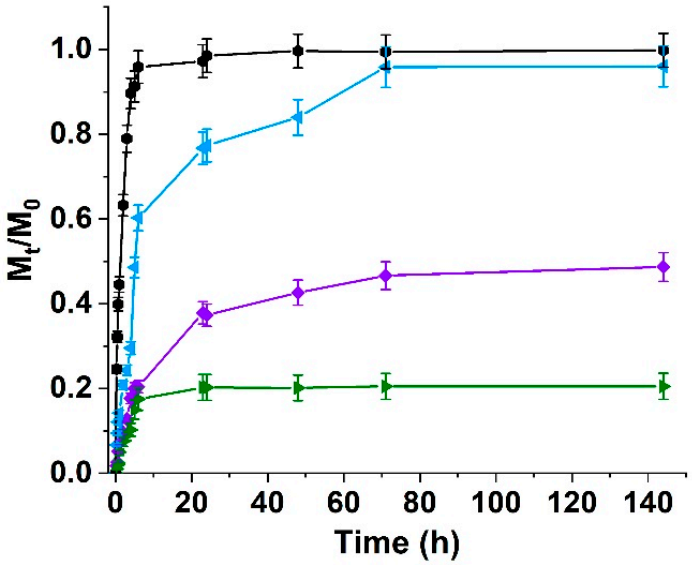

Figure 6. CUR release from H^C_{A-GO} at 0 (purple line), 12 (cyan line), 24 (green line), and 48 (black line) V.

As extensively explained elsewhere [46,53], the external voltage carried out a perturbation of the drug-to-carrier interactions, resulting in higher and faster release at 12 vs. 0 V. On the other hand, a further increase in the applied voltage (24 V) resulted in more pronounced hydrogel deformation and polarization, which were responsible for an apparent improvement of the CUR affinity and a consequent reduction of M_t/M_0 at 144 h value to 0.20. Detailed kinetic parameters were reported in Table 4.

Table 4. Kinetic parameters for CUR release from hybrid H^C_{A-GO} and blank H^C_A hydrogels upon application of external voltages at 12, 24, and 48 V.

Hydrogel	Voltage	Zero Order		First Order		Ritger-Peppas			Peppas-Sahlin				
		R^2	k_1 (10^{-2})	R^2	k_2	R^2	k_P	n	R^2	m	k'_S	k''_S (10^{-2})	$\frac{k'_S}{k''_S}$
H^C_A	12	0.555	1.08	0.993	0.18	0.926	0.32	0.27	0.967	0.48	0.27	1.67	16
	24	0.567	1.08	0.991	0.17	0.931	0.31	0.28	0.961	0.49	0.26	1.54	17
	48	0.549	1.09	0.987	0.19	0.905	0.34	0.26	0.973	0.46	0.29	2.03	14
H^C_{A-GO}	12	0.635	0.97	0.969	0.14	0.909	0.24	0.31	0.963	0.51	0.20	0.97	21
	24	0.518	0.23	0.986	0.23	0.901	0.07	0.25	0.921	0.45	0.07	0.49	14
	48	0.405	1.11	0.984	0.62	0.914	0.15	0.57	0.915	0.32	0.62	8.83	7

As expected, the control H^C_A was found to be not affected by the electric stimulation due to the absence of any conductive element in its composition. The hybrid H^C_{A-GO} samples showed a marked dependence of the release kinetics on the applied voltage. An electric field of 12 V resulted in an enhancement of releasing rate (k_P almost doubled from 0.11 to 0.24), due to both hydrogels swelling and perturbation of the drug-to-carrier interaction as a consequence of polarization phenomena. At 24 V, a marked reduction of the drug release occurred, probably as a result of the re-arrangement of the interaction forces. Finally, the application of the highest tested voltage (48 V) resulted in a significant jump in the kinetics due to the establishment of strong repulsive forces between ionized Alg residues and polarized CUR. The different behavior recorded in the swelling and release

assays were further proved by considering the Peppas-Sahlin parameters, indicating that the increase in the applied voltages carried out more significant anomalous diffusion phenomena (reduced $\frac{k'_S}{k''_S}$ values), thus confirming that the electric stimulation affected the drug release mainly modulating the drug-to-carrier interactions.

To clearly assess the latter statement, we performed a CUR release experiment under changeable voltage (Figure 7). In detail, the selected protocol involved a preliminary (1 h) incubation of loaded H^C_{A-GO} sample at 0 V, followed by the application of the electric field hypothesized to promote the highest CUR release (48 V, 1h). As expected, the amount of released CUR jumped from 7 to 70%, with the removal of the electric stimulation responsible for only a further 5% release in the subsequent 2 h. Finally, if the 48 V stimulation is re-established, an almost complete release of the therapeutic agent was reached.

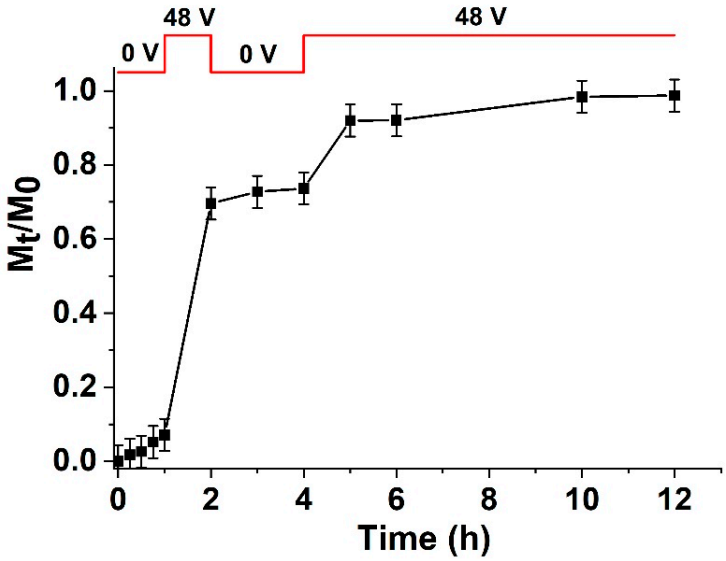

Figure 7. CUR release from H^C_{A-GO} under changeable voltage: 0 V (1 h), 48 V (1 h), 0 V (2 h), and 48 V (8 h).

4. Conclusions

In this study, we presented experimental evidence that the crosslinking method greatly affected the releasing performance of hybrid hydrogels composed of sodium alginate (Alg) and graphene oxide (GO).

Two synthetic approaches were used, namely the Ca^{2+} induced gelation (physical hydrogels, H^P_{A-GO}) and the radical co-polymerization (chemical hydrogels, H^C_{A-GO}) in the presence of acrylate monomers/crosslinkers such as hydroxyethyl acrylate (HEA) and polyethylene glycol dimethacrylate 750 (PEGDMA) as plasticizer and crosslinker, respectively. It was found that the ionic gelation allowed the homogeneous incorporation of 2.0% amount (by weight) of GO, while this value is reduced to 1.15% for H^C_{A-GO} due to the chain terminating effect GO. The evaluation of thermal properties clearly proved that higher thermal stability was conferred by the chemical crosslinking compared to the ionic gelation (main weight losses at 413 and 297 °C for H^C_{A-GO} and H^P_{A-GO}, respectively). The insertion of GO within the polymer network was carried out on an enhancement of swelling degree in both cases, probably as a consequence of the interference of carbon nanosheet with the crosslinking reactions. The presence of COOH within either the polysaccharide side chain or the carbon nanostructures was responsible for a higher swelling degree in physiological vs. acidic environments. Moreover, the water affinity of H^C_{A-GO} was found to be modulable by applying external voltages as a result of hydrogel deformation by combined ionization and osmotic pressure phenomena. This effect cannot be measured in H^P_{A-GO}, since in this case the movement of ionic species towards the appositively charged electrodes enhanced the hydrogel de-crosslinking by replacement of Ca^{2+} with Na^+ ions.

The determination of delivery performances was performed by using Curcumin as model therapeutics, loaded at 2.5 and 7.5% into H^{P}_{A-GO} and H^{C}_{A-GO}, respectively. These amounts represented the loading value allowing sustained releasing profiles: higher amounts into H^{C}_{A-GO} resulted in burst release, while no significant amount of CUR was found in the releasing media when a low amount of the bioactive agent was loaded into H^{C}_{A-GO}. The release was faster in H^{P}_{A-GO} than in H^{C}_{A-GO}, highlighting that the release is a complex phenomenon that cannot be exclusively related to the hydrogel water affinity. More interestingly, H^{C}_{A-GO} was able to modulate the release (in terms of both amount and rate) upon application of electric stimulation, with the combination of polarization and swelling variation phenomena carrying out to enhanced or reduced release.

Taken together, the results here reported proved that different synthetic approaches allowed the obtainment of materials with different performances, which can be useful to match different therapeutic needs. Further experiments need to be performed to prove that, although the mechanical characterization was not assessed, samples can be used for the preparation of skin patches with tailored performances useful for different therapeutic outcomes in the case of in vitro and, eventually, in the case of in vivo models.

Author Contributions: Conceptualization, L.F.M., S.H, and G.C.; methodology, F.P.N. and G.C.; validation, F.I. and G.C.; formal analysis, M.C. and F.I.; investigation, L.F.M. and M.C.; resources, S.H.; data curation, F.I. and F.P.N.; writing—original draft preparation, L.F.M. and G.C.; writing—review and editing, F.I., F.P.N. and S.H.; visualization, M.C.; supervision, S.H. and G.C.; funding acquisition, S.H. All authors have read and agreed to the published version of the manuscript.

Funding: This research received no external funding. M.C. is funded by PON R&I 2014–2020 Azione IV.6—"Contratti di ricerca su tematiche Green".

Institutional Review Board Statement: Not applicable.

Informed Consent Statement: Not applicable.

Data Availability Statement: Data are contained within the article.

Conflicts of Interest: The authors declare no conflict of interest.

References

1. Chen, B.Q.; Dragomir, M.P.; Yang, C.; Li, Q.Q.; Horst, D.; Calin, G.A. Targeting non-coding RNAs to overcome cancer therapy resistance. *Signal Transduct. Target. Ther.* **2022**, *7*, 121. [CrossRef] [PubMed]
2. Lei, W.; Yang, C.; Wu, Y.; Ru, G.Q.; He, X.L.; Tong, X.M.; Wang, S.B. Nanocarriers surface engineered with cell membranes for cancer targeted chemotherapy. *J. Nanobiotechnol.* **2022**, *20*, 45. [CrossRef] [PubMed]
3. Makharza, S.A.; Cirillo, G.; Vittorio, O.; Valli, E.; Voli, F.; Farfalla, A.; Curcio, M.; Lemma, F.; Nicoletta, F.P.; El-Gendy, A.A.; et al. Magnetic Graphene Oxide Nanocarrier for Targeted Delivery of Cisplatin: A Perspective for Glioblastoma Treatment. *Pharmaceuticals* **2019**, *12*, 76. [CrossRef] [PubMed]
4. Oh, J.S.; Lee, E.J. Photodynamic Graphene Oxide Combined Alginate Hydrogel for Controlled Drug Release. *Macromol. Res.* **2021**, *29*, 383–390. [CrossRef]
5. Curcio, M.; Brindisi, M.; Cirillo, G.; Frattaruolo, L.; Leggio, A.; Rago, V.; Nicoletta, F.P.; Cappello, A.R.; Iemma, F. Smart Lipid-Polysaccharide Nanoparticles for Targeted Delivery of Doxorubicin to Breast Cancer Cells. *Int. J. Mol. Sci.* **2022**, *23*, 2386. [CrossRef]
6. Islam, M.S.; Renner, F.; Azizighannad, S.; Mitra, S. Direct incorporation of nano graphene oxide (nGO) into hydrophobic drug crystals for enhanced aqueous dissolution. *Colloids Surf. B Biointerfaces* **2020**, *189*, 110827. [CrossRef] [PubMed]
7. Priyadarsini, S.; Mohanty, S.; Mukherjee, S.; Basu, S.; Mishra, M. Graphene and graphene oxide as nanomaterials for medicine and biology application. *J. Nanostruct. Chem.* **2018**, *8*, 123–137. [CrossRef]
8. Curcio, M.; Farfalla, A.; Saletta, F.; Valli, E.; Pantuso, E.; Nicoletta, F.P.; Iemma, F.; Vittorio, O.; Cirillo, G. Functionalized Carbon Nanostructures Versus Drug Resistance: Promising Scenarios in Cancer Treatment. *Molecules* **2020**, *25*, 2102. [CrossRef] [PubMed]
9. di Luca, M.; Vittorio, O.; Cirillo, G.; Curcio, M.; Czuban, M.; Voli, F.; Farfalla, A.; Hampel, S.; Nicoletta, F.P.; Iemma, F. Electro-responsive graphene oxide hydrogels for skin bandages: The outcome of gelatin and trypsin immobilization. *Int. J. Pharm.* **2018**, *546*, 50–60. [CrossRef]
10. Ligorio, C.; O'Brien, M.; Hodson, N.W.; Mironov, A.; Iliut, M.; Miller, A.F.; Vijayaraghavan, A.; Hoyland, J.A.; Saiani, A. TGF-P3-loaded graphene oxide—Self-assembling peptide hybrid hydrogels as functional 3D scaffolds for the regeneration of the nucleus pulposus. *Acta Biomater.* **2021**, *127*, 116–130. [CrossRef]

11. Chung, S.; Revia, R.A.; Zhang, M.Q. Graphene Quantum Dots and Their Applications in Bioimaging, Biosensing, and Therapy. *Adv. Mater.* **2021**, *33*, 1904362. [CrossRef] [PubMed]
12. Radic, M.B.M.; Filipovic, V.V.; Vukomanovic, M.; Runic, J.N.; Tomic, S.L. Degradable 2-Hydroxyethyl Methacrylate/Gelatin/Alginate Hydrogels Infused by Nanocolloidal Graphene Oxide as Promising Drug Delivery and Scaffolding Biomaterials. *Gels* **2022**, *8*, 22. [CrossRef] [PubMed]
13. Liu, M.; Zeng, X.; Ma, C.; Yi, H.; Ali, Z.; Mou, X.B.; Li, S.; Deng, Y.; He, N.Y. Injectable hydrogels for cartilage and bone tissue engineering. *Bone Res.* **2017**, *5*, 17014. [CrossRef] [PubMed]
14. Zhao, X.; Wu, H.; Guo, B.L.; Dong, R.N.; Qiu, Y.S.; Ma, P.X. Antibacterial anti-oxidant electroactive injectable hydrogel as self-healing wound dressing with hemostasis and adhesiveness for cutaneous wound healing. *Biomaterials* **2017**, *122*, 34–47. [CrossRef] [PubMed]
15. Fan, F.; Saha, S.; Hanjaya-Putra, D. Biomimetic Hydrogels to Promote Wound Healing. *Front. Bioeng. Biotechnol.* **2021**, *9*, 718377. [CrossRef]
16. Liang, Y.P.; He, J.H.; Guo, B.L. Functional Hydrogels as Wound Dressing to Enhance Wound Healing. *ACS Nano* **2021**, *15*, 12687–12722. [CrossRef]
17. Qu, J.; Zhao, X.; Liang, Y.P.; Zhang, T.L.; Ma, P.X.; Guo, B.L. Antibacterial adhesive injectable hydrogels with rapid self-healing, extensibility and compressibility as wound dressing for joints skin wound healing. *Biomaterials* **2018**, *183*, 185–199. [CrossRef]
18. Stan, D.; Tanase, C.; Avram, M.; Apetrei, R.; Mincu, N.B.; Mateescu, A.L.; Stan, D. Wound healing applications of creams and "smart" hydrogels. *Exp. Dermatol.* **2021**, *30*, 1218–1232. [CrossRef]
19. Liu, H.; Wang, C.Y.; Li, C.; Qin, Y.G.; Wang, Z.H.; Yang, F.; Li, Z.H.; Wang, J.C. A functional chitosan-based hydrogel as a wound dressing and drug delivery system in the treatment of wound healing. *RSC Adv.* **2018**, *8*, 7533–7549. [CrossRef]
20. di Luca, M.; Curcio, M.; Valli, E.; Cirillo, G.; Voli, F.; Butini, M.E.; Farfalla, A.; Pantuso, E.; Leggio, A.; Nicoletta, F.P.; et al. Combining antioxidant hydrogels with self-assembled microparticles for multifunctional wound dressings. *J. Mater. Chem. B* **2019**, *7*, 4361–4370. [CrossRef]
21. Li, J.Y.; Mooney, D.J. Designing hydrogels for controlled drug delivery. *Nat. Rev. Mater.* **2016**, *1*, 16071. [CrossRef] [PubMed]
22. Hu, W.K.; Wang, Z.J.; Xiao, Y.; Zhang, S.M.; Wang, J.L. Advances in crosslinking strategies of biomedical hydrogels. *Biomater. Sci.* **2019**, *7*, 843–855. [CrossRef]
23. Zhao, X.; Liang, Y.P.; Huang, Y.; He, J.H.; Han, Y.; Guo, B.L. Physical Double-Network Hydrogel Adhesives with Rapid Shape Adaptability, Fast Self-Healing, Antioxidant and NIR/pH Stimulus-Responsiveness for Multidrug-Resistant Bacterial Infection and Removable Wound Dressing. *Adv. Funct. Mater.* **2020**, *30*, 1910748. [CrossRef]
24. Li, M.; Liang, Y.P.; He, J.H.; Zhang, H.L.; Guo, B.L. Two-Pronged Strategy of Biomechanically Active and Biochemically Multifunctional Hydrogel Wound Dressing To Accelerate Wound Closure and Wound Healing. *Chem. Mater.* **2020**, *32*, 9937–9953. [CrossRef]
25. Zheng, W.; Wang, L.; Jiao, H.; Wu, Z.; Zhao, Q.; Lin, T.; Ma, H.; Zhang, Z.; Xu, X.; Cao, J.; et al. A cost-effective, fast cooling, and efficient anti-inflammatory multilayered topological hydrogel patch for burn wound first aid. *Chem. Eng. J.* 2022; *in press*. [CrossRef]
26. Zhao, Q.; Liu, J.Y.; Wu, Z.X.; Xu, X.Y.; Ma, H.D.; Hou, J.; Xu, Q.L.; Yang, R.P.; Zhang, K.Y.; Zhang, M.M.; et al. Robust PEDOT:PSS-based hydrogel for highly efficient interfacial solar water purification. *Chem. Eng. J.* **2022**, *442*, 136284. [CrossRef]
27. Aparicio-Collado, J.L.; Garcia-San-Martin, N.; Molina-Mateo, J.; Cabanilles, C.T.; Quiles, V.D.; Serrano-Aroca, A.; Serra, R.S.I. Electroactive calcium-alginate/polycaprolactone/reduced graphene oxide nanohybrid hydrogels for skeletal muscle tissue engineering. *Colloidc Surf. B Biointerfaces* **2022**, *214*, 112455. [CrossRef]
28. Garcia-Couce, J.; Vernhes, M.; Bada, N.; Aguero, L.; Valdes, O.; Alvarez-Barreto, J.; Fuentes, G.; Almirall, A.; Cruz, L.J. Synthesis and Evaluation of AlgNa-g-Poly(QCL-co-HEMA) Hydrogels as Platform for Chondrocyte Proliferation and Controlled Release of Betamethasone. *Int. J. Mol. Sci.* **2021**, *22*, 5730. [CrossRef] [PubMed]
29. Sengupta, I.; Kumar, S.S.S.S.; Gupta, K.; Chakraborty, S. In-vitro release study through novel graphene oxide aided alginate based pH-sensitive drug carrier for gastrointestinal tract. *Mater. Today Commun.* **2021**, *26*, 101737. [CrossRef]
30. Geng, Z.J.; Ji, Y.X.; Yu, S.; Liu, Q.F.; Zhou, Z.B.; Guo, C.P.; Lu, D.H.; Pei, D.T. Preparation and characterization of a dual cross-linking injectable hydrogel based on sodium alginate and chitosan quaternary ammonium salt. *Carbohydr. Res.* **2021**, *507*, 108389. [CrossRef]
31. Wang, L.N.; Zhang, H.J.; Liu, X.Q.; Liu, Y.; Zhu, X.; Liu, X.H.; You, X.Y. A Physically Cross-Linked Sodium Alginate-Gelatin Hydrogel with High Mechanical Strength. *ACS Appl. Polym. Mater.* **2021**, *3*, 3197–3205. [CrossRef]
32. Sanchez-Fernandez, J.A.; Presbitero-Espinosa, G.; Pena-Paras, L.; Pizana, E.I.R.; Galvan, K.P.V.; Vopalensky, M.; Kumpova, I.; Elizalde-Herrera, L.E. Characterization of Sodium Alginate Hydrogels Reinforced with Nanoparticles of Hydroxyapatite for Biomedical Applications. *Polymers* **2021**, *13*, 2927. [CrossRef] [PubMed]
33. Theodorakis, N.; Saravanou, S.F.; Kouli, N.P.; Iatridi, Z.; Tsitsilianis, C. pH/Thermo-Responsive Grafted Alginate-Based SiO_2 Hybrid Nanocarrier/Hydrogel Drug Delivery Systems. *Polymers* **2021**, *13*, 1228. [CrossRef]
34. Shahriari-Khalaji, M.; Hong, S.Y.; Hu, G.Q.; Ji, Y.; Hong, F.F. Bacterial Nanocellulose-Enhanced Alginate Double-Network Hydrogels Cross-Linked with Six Metal Cations for Antibacterial Wound Dressing. *Polymers* **2020**, *12*, 2683. [CrossRef]
35. Wang, Q.Q.; Liu, Y.; Zhang, C.J.; Zhang, C.; Zhu, P. Alginate/gelatin blended hydrogel fibers cross-linked by Ca^{2+} and oxidized starch: Preparation and properties. *Mat. Sci. Eng. C* **2019**, *99*, 1469–1476. [CrossRef] [PubMed]

36. Raja, C.A.; Balakumar, S.; Anandkumar, B.; George, R.P.; Mudali, U.K. Formation of bioactive nano hybrid thin films on anodized titanium via electrophoretic deposition intended for biomedical applications. *Mater. Today Commun.* **2020**, *25*, 101666. [CrossRef]
37. Devi, G.V.Y.; Prabhu, A.; Anil, S.; Venkatesan, J. Preparation and characterization of dexamethasone loaded sodium alginate-graphene oxide microspheres for bone tissue engineering. *J. Drug Deliv. Sci. Technol.* **2021**, *64*, 102624. [CrossRef]
38. Abasalizadeh, F.; Moghaddam, S.V.; Alizadeh, E.; Akbari, E.; Kashani, E.; Fazljou, S.M.B.; Torbati, M.; Akbarzadeh, A. Alginate-based hydrogels as drug delivery vehicles in cancer treatment and their applications in wound dressing and 3D bioprinting. *J. Biol. Eng.* **2020**, *14*, 8. [CrossRef] [PubMed]
39. Khan, M.U.A.; Abd Razak, S.I.; Haider, S.; Mannan, H.A.; Hussain, J.; Hasan, A. Sodium alginate-f-GO composite hydrogels for tissue regeneration and antitumor applications. *Int. J. Biol. Macromol.* **2022**, *208*, 475–485. [CrossRef] [PubMed]
40. Yun, Y.J.; Wu, H.W.; Gao, J.; Dai, W.; Deng, L.H.; Lv, O.; Kong, Y. Facile synthesis of Ca^{2+}-crosslinked sodium alginate/graphene oxide hybrids as electro- and pH-responsive drug carrier. *Mat. Sci. Eng. C* **2020**, *108*, 110380. [CrossRef] [PubMed]
41. Lentz, L.; Mayer, D.A.; Dogenski, M.; Ferreira, S.R.S. Hybrid aerogels of sodium alginate/graphene oxide as efficient adsorbents for wastewater treatment. *Mater. Chem. Phys.* **2022**, *283*, 125981. [CrossRef]
42. Jin, Y.; Zhang, W.K.; Zhang, Y.H.; Yang, Y.Q.; Fang, Z.W.; Song, J.L.; Qian, Y.; Yuan, W.E. Multifunctional biomimetic hydrogel based on graphene nanoparticles and sodium alginate for peripheral nerve injury therapy. *Biomater. Adv.* **2022**, *135*, 212727. [CrossRef]
43. Khapre, M.A.; Pandey, S.; Jugade, R.M. Glutaraldehyde-cross-linked chitosan-alginate composite for organic dyes removal from aqueous solutions. *Int. J. Biol. Macromol.* **2021**, *190*, 862–875. [CrossRef]
44. Fan, L.H.; Ge, H.Y.; Zou, S.Q.; Xiao, Y.; Wen, H.H.; Li, Y.; Feng, H.; Nie, M. Sodium alginate conjugated graphene oxide as a new carrier for drug delivery system. *Int. J. Biol. Macromol.* **2016**, *93*, 582–590. [CrossRef] [PubMed]
45. Serrano-Aroca, A.; Ferrandis-Montesinos, M.; Wang, R.B. Antiviral Properties of Alginate-Based Biomaterials: Promising Antiviral Agents against SARS-CoV-2. *ACS Appl. Bio Mater.* **2021**, *4*, 5897–5907. [CrossRef]
46. Cirillo, G.; Pantuso, E.; Curcio, M.; Vittorio, O.; Leggio, A.; Iemma, F.; De Filpo, G.; Nicoletta, F.P. Alginate Bioconjugate and Graphene Oxide in Multifunctional Hydrogels for Versatile Biomedical Applications. *Molecules* **2021**, *26*, 1355. [CrossRef] [PubMed]
47. Madeo, L.F.; Sarogni, P.; Cirillo, G.; Vittorio, O.; Voliani, V.; Curcio, M.; Shai-Hee, T.; Buchner, B.; Mertig, M.; Hampel, S. Curcumin and Graphene Oxide Incorporated into Alginate Hydrogels as Versatile Devices for the Local Treatment of Squamous Cell Carcinoma. *Materials* **2022**, *15*, 1648. [CrossRef] [PubMed]
48. Shen, J.; Burgess, D.J. In vitro dissolution testing strategies for nanoparticulate drug delivery systems: Recent developments and challenges. *Drug Deliv. Transl. Res.* **2013**, *3*, 409–415. [CrossRef]
49. Zaborniak, I.; Chmielarz, P. Comestible curcumin: From kitchen to polymer chemistry as a photocatalyst in metal-free ATRP of (meth)acrylates. *J. Ind. Eng. Chem.* **2022**, *105*, 481–490. [CrossRef]
50. Zheng, H.C.; Yang, J.S.; Han, S.Y. The synthesis and characteristics of sodium alginate/graphene oxide composite films crosslinked with multivalent cations. *J. Appl. Polym. Sci.* **2016**, *133*, 43616. [CrossRef]
51. Yong, Q.W.; Liang, C.Z. Synthesis of an Aqueous Self-Matting Acrylic Resin with Low Gloss and High Transparency via Controlling Surface Morphology. *Polymers* **2019**, *11*, 322. [CrossRef]
52. Wallmersperger, T.; Ballhause, D.; Kroplin, B. On the modeling of polyelectrolyte gels. *Macromol. Symp.* **2007**, *254*, 306–313. [CrossRef]
53. Cirillo, G.; Curcio, M.; Spizzirri, U.G.; Vittorio, O.; Tucci, P.; Picci, N.; Iemma, F.; Hampel, S.; Nicoletta, F.P. Carbon nanotubes hybrid hydrogels for electrically tunable release of Curcumin. *Eur. Polym. J.* **2017**, *90*, 1–12. [CrossRef]
54. Talebian, S.; Mehrali, M.; Raad, R.; Safaei, F.; Xi, J.T.; Liu, Z.F.; Foroughi, J. Electrically Conducting Hydrogel Graphene Nanocomposite Biofibers for Biomedical Applications. *Front. Chem.* **2020**, *8*, 88. [CrossRef]
55. Saikia, A.K.; Aggarwal, S.; Mandal, U.K. Electrically induced swelling and methylene blue release behaviour of poly (*N*-isopropylacrylamide-co-acrylamido-2-methylpropyl sulphonic acid) hydrogels. *Colloid Polym. Sci.* **2015**, *293*, 3533–3544. [CrossRef]
56. Wanjale, M.V.; Jaikumar, V.S.; Sivakumar, K.C.; Paul, R.A.; James, J.; Kumar, G.S.V. Supramolecular Hydrogel Based Post-Surgical Implant System for Hydrophobic Drug Delivery Against Glioma Recurrence. *Int. J. Nanomed.* **2022**, *17*, 2203–2224. [CrossRef] [PubMed]
57. Kalepu, S.; Nekkanti, V. Insoluble drug delivery strategies: Review of recent advances and business prospects. *Acta Pharm. Sin. B* **2015**, *5*, 442–453. [CrossRef] [PubMed]
58. Reis, A.V.; Guilherme, M.R.; Rubira, A.F.; Muniz, E.C. Mathematical model for the prediction of the overall profile of in vitro solute release from polymer networks. *J. Colloid Interface Sci.* **2007**, *310*, 128–135. [CrossRef]
59. Siepmann, J.; Gopferich, A. Mathematical modeling of bioerodible, polymeric drug delivery systems. *Adv. Drug Deliv. Rev.* **2001**, *48*, 229–247. [CrossRef] [PubMed]
60. Malekjani, N.; Jafari, S.M. Modeling the release of food bioactive ingredients from carriers/nanocarriers by the empirical, semiempirical, and mechanistic models. *Compr. Rev. Food Sci. Food Saf.* **2021**, *20*, 3–47. [CrossRef]
61. Unagolla, J.M.; Jayasuriya, A.C. Drug transport mechanisms and in vitro release kinetics of vancomycin encapsulated chitosan-alginate polyelectrolyte microparticles as a controlled drug delivery system. *Eur. J. Pharm. Sci.* **2018**, *114*, 199–209. [CrossRef]

62. Li, X.S.; Li, Q.; Zhao, C. Zero-Order Controlled Release of Water-Soluble Drugs Using a Marker Pen Platform. *ACS Omega* **2021**, *6*, 13774–13778. [CrossRef] [PubMed]
63. Fu, Y.; Kao, W.J. Drug release kinetics and transport mechanisms of non-degradable and degradable polymeric delivery systems. *Expert Opin. Drug Deliv.* **2010**, *7*, 429–444. [CrossRef] [PubMed]
64. Sulttan, S.; Rohani, S. Controlled Drug Release of Smart Magnetic Self-Assembled Micelle, Kinetics and Transport Mechanisms. *J. Pharm. Sci.* **2022**, *111*, 2378–2388. [CrossRef] [PubMed]